AIP | Journal of Applied Physics

Kinetic transition in the growth of Al nanocrystals in Al-Sm alloys

S. D. Imhoff, J. Ilavsky, F. Zhang, P. Jemian, P. G. Evans et al.

Citation: J. Appl. Phys. **111**, 063525 (2012); doi: 10.1063/1.3697654
View online: http://dx.doi.org/10.1063/1.3697654
View Table of Contents: http://jap.aip.org/resource/1/JAPIAU/v111/i6
Published by the American Institute of Physics.

Kinetic transition in the growth of Al nanocrystals in Al-Sm alloys

S. D. Imhoff,[1] J. Ilavsky,[2] F. Zhang,[2,a)] P. Jemian,[2] P. G. Evans,[1,b)] and J. H. Perepezko[1,c)]
[1]*Department of Materials Science and Engineering, University of Wisconsin-Madison, 1509 University Ave., Madison, Wisconsin 53706, USA*
[2]*Advanced Photon Source, Argonne National Laboratory, 9700 S. Cass Ave., Argonne, Illinois 60439, USA*

(Received 27 January 2012; accepted 22 February 2012; published online 29 March 2012)

The formation of Al nanocrystals from an amorphous $Al_{92}Sm_8$ alloy involves kinetic phenomena with very different characteristic length and timescales, including initial nucleation and later growth and coarsening. Insight into these processes can be derived from the evolution of the sizes of nanocrystals as a function of time. Synchrotron small angle x-ray scattering (SAXS) experiments provide information about the evolution of the nanocrystal size distribution, particularly at times after nucleation has reached saturation. Accurately interpreting the distribution of intensity measured using SAXS requires a nanoparticle model consisting of nanocrystalline core of pure Al surrounded by a shell enriched in Sm. With this approach, statistical parameters derived from SAXS are independent of detailed assumptions regarding the distribution of Sm around the nanocrystals and allow the maximum radius of nanocrystals within the distribution to be determined unambiguously. Sizes determined independently using transmission electron microcopy are in excellent agreement with the SAXS results. The maximum radius obtained from SAXS is proportional to the cube root of time at large sizes and long times, consistent with a coarsening model. The diffusivity of Al within the Al-Sm alloy is obtained from a quantitative analysis of the coarsening process. Further analysis with this diffusivity and a particle growth model provides a satisfactory account for the particle size evolution at early times before the kinetic transition to coarsening. © *2012 American Institute of Physics*. [http://dx.doi.org/10.1063/1.3697654]

I. INTRODUCTION

Composites formed via the growth of nanocrystals within an amorphous metallic alloy have novel properties including extremely high mechanical strength.[1] The most desirable properties for mechanical applications are obtained by partial crystallization resulting in the creation of pure Al nanocrystals with number densities of 10^{20} to 10^{24} m^{-3}.[1,2] The desired crystal population can be introduced by quenching the alloy from the homogeneous liquid, commonly an aluminum-rare earth alloy, into a fully amorphous state followed by subsequent annealing above room temperature. It is difficult to develop predictive models of the nanocrystal development during this isothermal devitrification process because the growth involves a series of mechanisms which are not easily separated from one another. The complicated kinetics of these mechanisms makes assessment of the relevant parameters challenging.[3] The present experimental study is focused on the growth of nanocrystals within amorphous Al-Sm alloys during annealing times after nucleation saturation is reached and when coarsening controls the sizes of particles. The long-time behavior of the particle population can also be used to gain insight into the initial growth kinetics before the kinetic transition in the evolution of the nanocrystal sizes from diffusion-limited growth at short times to coarsening at longer times.

The nanocrystal size distributions were obtained using small angle x-ray scattering (SAXS) and transmission electron microscopy (TEM). In analyzing the SAXS data it is essential to consider the redistribution of the rare-earth solute around Al nanocrystals. The key issue is that Al nanoparticles can grow only by moving Sm atoms out of the volume occupied by the nanocrystal. The precipitates thus consist of a pure Al nanocrystal surrounded by a region enriched in Sm. The overall precipitate, including both the nanocrystal and the Sm-rich shell, has zero net density difference with respect to the Al-Sm alloy. This poses a particular challenge to scattering experiments in that the combined scattering power of the growing nanocrystal and the shell surrounding it closely match the amorphous matrix. This problem is solved by analyzing the distribution of scattered intensity using a core-shell model. When interpreted in this way, SAXS provides an accurate measurement of the maximum size of nanocrystals. An alternative analysis using a spherical nanocrystal lacking such a shell has a net density difference with respect to the background and cannot fit the experimental results because it yields an intensity distribution with a maximum in scattered intensity at zero momentum transfer. Previous studies have found distributions of scattered intensity similar to those reported here, and explained peaks in these distributions by invoking a distribution of spatially correlated spherical scatterers.[4] The present results and models show that no such correlation is necessary to explain the scattering results. The analysis of the SAXS data using the core-shell model of growing nanocrystals includes two

[a)]Present address: National Institute of Standards and Technology, 100 Bureau Dr., Gaithersburg, MD 20899, USA.
[b)]Electronic mail: evans@engr.wisc.edu.
[c)]Electronic mail: perepezk@engr.wisc.edu.

numerical strategies for that can be used to determine the size of the nanocrystals.

The SAXS approach is applied to determine the nanocrystal size distribution in Al-Sm samples annealed at temperatures from 120 to 140 °C for times up to 24 h. Results obtained by a quantitative analysis of TEM images at a series of annealing times at one of the temperatures are in excellent agreement with the SAXS results. A coarsening model describes the time dependence of the maximum sizes within the distribution. This model can then be used to determine the diffusivity of Al within the Al-Sm alloy. An extrapolation of the growth process to early times shows that a diffusion-limited growth mechanism, rather than coarsening, applies for times up to approximately 6 h at 130 °C.

II. EXPERIMENTAL DETAILS

Ribbons of $Al_{92}Sm_8$ metallic glass were formed by a single-roller melt spinning process, with a tangential wheel speed of 55 m s^{-1}. The initial alloy ingot was made by repeated arc melting of pure elemental components. Previous evaluation of these ribbons with TEM showed that annealing in an inert ultrahigh purity argon atmosphere resulted in the formation of Al crystals with diameters ranging from a few to tens of nanometers.[5] Crystallization upon heating results in a multistage reaction where first Al nanocrystals precipitate at temperatures of 100 to 200 °C and later an intermetallic phase consumes the remaining amorphous Al-Sm alloy at 250 to 300 °C.[5] These two reactions are apparent in the differential scanning calorimetry measurement shown in Fig. 1(a). Samples in the present study were annealed under isothermal conditions of 120 to 140 °C using a heating rate of 80 °C min^{-1} in the ramp-up period and a temperature overshoot of less than 0.5 °C. This process yields samples in which only the crystallization of Al has occurred with no formation of the intermetallic component. A cross sectional dark-field TEM image of a ribbon heated to 130 °C for 10 h is shown in Fig. 1(b). Al nanocrystals appear in dark-field TEM images as isolated regions in which there is either an excess or deficit of the intensity arising from diffraction of the incident beam by Bragg reflections of the Al crystallites.

Size distributions are obtained from TEM measurements by counting and measuring the radii of nanocrystals in dark-field images similar to the one shown in Fig. 1(b). The number density of nanocrystals is found by dividing the number of crystals by the volume sampled by the image. The dark-field measurement is repeated at a series of azimuthal angles around the ring of diffraction from the Al particles in order to account for the range of nanoparticle orientations. Sufficient counting statistics are obtained by counting the number of crystals in several images. The dark-field TEM studies are based on images using diffraction from Al and thus give the diameter of the Al nanocrystals but do not provide information about the composition gradient surrounding them. The TEM particle analysis was performed for ribbons annealed at 130 °C for 1, 3, 6, 8, and 10 h. A histogram of the radii of nanocrystals and the resulting cumulative probability distribution are shown in Fig. 1(c) for an Al-Sm sample annealed at 130 °C for 10 h.

X-ray scattering measurements were conducted using an ultra-small angle x-ray scattering instrument at the Advanced Photon Source of Argonne National Laboratory. This instrument uses a Bonse-Hart geometry to achieve extremely high resolution in reciprocal space and a large dynamic range in both intensity and scattering wavevector.[6,7] X-rays from an undulator insertion device passed through a two-crystal Si (111) premonochromator and then through a high resolution monochromator before striking the sample. Experiments were performed with a photon energy of 10.98 keV and an incident beam size of 2 mm × 400 μm. An analyzer in front of the detector selects radiation scattered to a narrow range of angles and eliminates the background that would arise from fluorescence radiation from the sample. The intensity of the scattered radiation was measured using a Si photodiode detector. This diode could be replaced with a charge coupled device (CCD) camera during the alignment to allow images to be made of the sources of scattering within the sample.

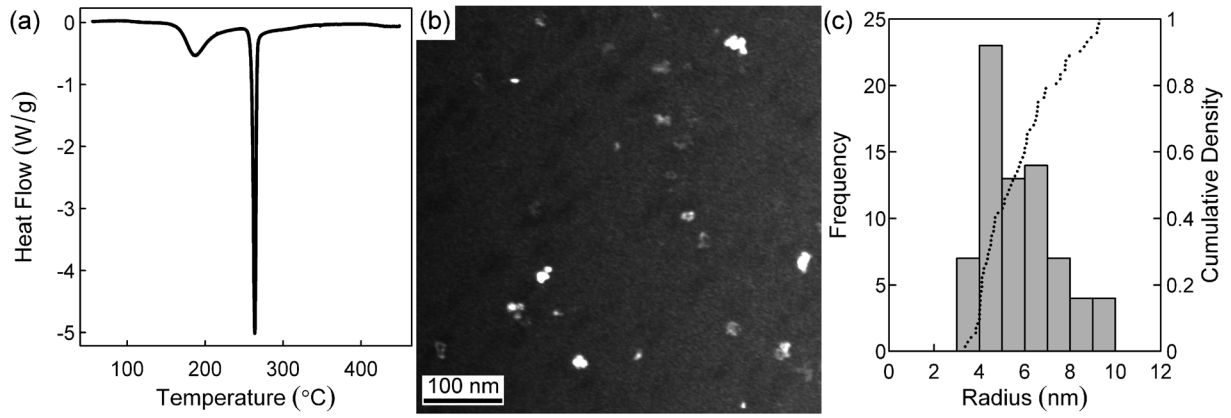

FIG. 1. (a) Differential scanning calorimetry measurement with a heating rate of 20 °C min^{-1} beginning with an as-spun $Al_{92}Sm_8$ amorphous ribbon. (b) Dark-field transmission electron micrograph of an Al-Sm amorphous alloy heated at 130 °C for 10 h. Nanocrystals that fulfill the Al (111) Bragg condition are visible as brighter features in the images. Other nanocrystalline areas extinguish the incident beam and lead to dark regions. (c) Histogram and the cumulative probability distribution function for the radii of Al nanocrystals in an Al-Sm amorphous alloy heated to 130 °C for 10 h, obtained using transmission electron microscopy.

The samples for x-ray scattering experiments consisted of stacks of several foils of Al-Sm alloy ribbon such that the total thickness of the stack matched the incident beam absorption length of approximately 50 μm. In some samples it was found that large-scale mechanical deformations produced spatially localized regions of high x-ray scattering intensity. This scattering was due to large mechanical defects, including the edges, voids, and cracks, and was associated with the large discontinuity in electron density at these features. CCD images of the spatial distribution of the scattered x-rays were useful in selecting areas of the sample for which the intensity was uniformly distributed and representative of the formation of nanocrystals.

The SAXS intensity distributions were acquired by measuring the intensity at a series of scattering angles chosen to achieve a uniform density of points along a logarithmic axis in reciprocal space. The one-dimensional collimated geometry under which the USAXS instrument was operated leads to a slit-smearing effect that broadened features in reciprocal space. A desmearing algorithm was employed to remove this effect before analyzing the data.[8]

III. MODELS FOR SMALL ANGLE X-RAY SCATTERING

A. Particle description

The SAXS intensity distributions were interpreted using a core-shell model for the distribution of Al and Sm atoms in the Al nanocrystals and the surrounding region rich in Sm. The model is based on the negligible solubility of Sm in crystalline Al that results in the displacement of Sm during the growth into a shell surrounding the Al nanocrystal. It is further assumed that the rejected Sm remains in the shell rather than mixing back into the background of amorphous Al-Sm alloy, due to the slow diffusion of large rare earth atoms. To simplify the model, the Sm-rich shell surrounding the crystal is considered to have a homogenous concentration of Sm, resulting in the core-shell structures shown in Fig. 2(a). The pure-Al core with radius R_c is surrounded by a shell enriched in Sm with radius R_s.

Previous studies have used similar core-shell models to describe the redistribution of the alloy components around a precipitate, and in turn have used this distribution to understand diffusive transport in precipitation problems.[9,10] Hermann *et al.* modeled the growth of nanocrystals in a $Zr_{41}Be_{22.5}Ti_{14}Cu_{12.5}Ni_{10}$ alloy, assuming an exponentially decaying difference in composition and scattering density with respect to the alloy outside the particle.[9] Lembke *et al.* applied a similar model of the composition distribution to particles in a glass ceramic.[10] As in the present case, the average density of the precipitate/shell systems in Refs. 9 and 10 were identical to the background. In the present work, however, the core-shell model is modified slightly to use a constant Sm composition in the shell in order to simplify the calculation.

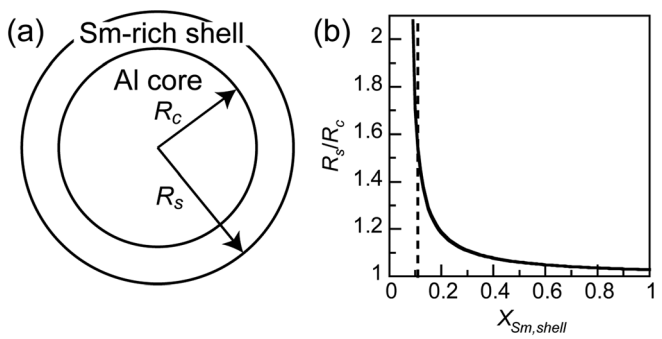

FIG. 2. (a) The core-shell model used to interpret the small angle x-ray scattering measurements. A core of pure Al with radius R_c is surrounded by a shell of radius R_s enriched in Sm. (b) The ratio of the radii of the shell and core as a function of $X_{Sm,shell}$, assuming an initial alloy composition $X_{Sm,alloy} = 8\%$. The vertical line indicates the composition expected from thermodynamic predictions, $X_{Sm,shell} = 11\%$.

The atomic fractions of Sm in the shell and the starting alloy are $X_{Sm,shell}$ and $X_{Sm,alloy}$, respectively. With the assumption that the total concentration N_t of atoms is constant, the number of Sm atoms displaced from a core of radius R_c is $N_t X_{Sm,alloy}(4/3)\pi R_c^3$. All of the displaced Sm atoms add to the Sm concentration in the shell. The number of additional Sm atoms, beyond those that would already be found in the Al-Sm alloy, that can be accommodated in a shell of inner radius R_c and outer radius R_s is $N_t(X_{Sm,shell} - X_{Sm,alloy})\,\frac{4}{3}\pi(R_s^3 - R_c^3)$. The number of Sm atoms displaced must be equal to the number added to the shell and R_s is thus

$$R_s = \left(\frac{X_{Sm,shell}}{X_{Sm,shell} - X_{Sm,alloy}}\right)^{1/3} R_c. \quad (1)$$

Equation (1) can be used to determine the radius of the shell that accompanies a pure Al core of radius R_c. A thermodynamic calculation extending the Al-Sm liquidus line below the equilibrium eutectic point predicts that $X_{Sm,shell} = 11\%$.[5] Only a relatively small atomic concentration of Sm can be thus added to the shell. As a result, in this range of compositions the radius of the Sm-rich shell is large with respect to the radius of the nanocrystal, as shown in the plot of the ratio of the radii of the shell and nanocrystalline core as a function of the shell composition in Fig. 2(b). The thermodynamically predicted shell composition gives $R_s = 1.54\,R_c$. As pointed out in Refs. 9 and 10, it is important to have an accurate model of this type of core-shell structure for small angle scattering experiments because the average electron density of this structure is identical to the background alloy.

B. Single-particle scattering model

The amplitude of the electric field of x-rays scattered to small angles by the core-shell structure associated with the nanocrystals can be found by computing the Fourier transform of its electron density distribution.[11] For this purpose, the Al nanocrystal/Al-Sm shell precipitate can be described as a set of N spherical shells with radii R_1 to R_N ordered from large to small and corresponding numbers of electrons per unit volume ρ_1 to ρ_N. The background electron density outside the largest shell is ρ_0. The present case has N=2. The scattering amplitude $A(q)$ for this set of shells is[12]

$$A(q) = \sum_{i=1}^{N} V(R_i)(\rho_i - \rho_{i-1}) f_1(q, R_i). \quad (2)$$

Here $A(q)$ is the scattering amplitude in units of electrons, where one electron corresponds to the electric field amplitude at wavevector q that would be equivalent to the scattering amplitude produced by one free electron.[11] The amplitude is expressed as a function of the scattering wavevector $q = 4\pi(\sin\theta/\lambda)$, where θ is one half of the angle between the incident and scattered beams of x-rays and λ is the x-ray wavelength. The volume of each shell is computed with $V(r) = (4/3)\pi r^3$, and $f_1(q,R)$ is the unitless scattering form factor for a sphere of radius R:[11]

$$f_1(q,R) = 3\frac{\sin qR - qR\cos qR}{(qR)^3}. \quad (3)$$

The electron densities of the shell, core, and amorphous Al-Sm alloy are ρ_s, ρ_c, and ρ_0, respectively. The scattering amplitude at wavevector q is

$$A_{\text{core-shell}}(q) = V(R_s)(\rho_s - \rho_c)f_1(q,R_s) + V(R_c)(\rho_c - \rho_o)f_1(q,R_c). \quad (4)$$

It is useful to compare the scattering from this core-shell structure with what would be observed for a sphere of uniform composition. The amplitude of scattering from a sphere of radius R_s and electron density ρ_s includes only a single term:

$$A_{\text{sphere}}(q) = V(R_s)(\rho_s - \rho_0)f_1(q,R_s). \quad (5)$$

The amplitudes for a sphere with $R_s = 10$ nm and a core-shell particle with $R_c = 10$ nm are shown in Fig. 3(a). The amplitudes in Fig. 3(a) are normalized independently to have the same peak value. The maximum of the scattering amplitude from the sphere is at $q = 0$, resulting from the change in the total electron density associated with the sphere.

The model corresponding to the Al nanocrystal/Sm-rich shell precipitate does not have a maximum at $q = 0$ because there is no zero-frequency component of the difference in the density between the core-shell structure and the remainder of the alloy. This effect has been described previously by Boucher *et al.* in small angle neutron scattering studies of $TbCu_{3.54}$.[13] A similar phenomenon can be expected in any system where precipitates form with a composition that is distinct from the matrix, and in which the excluded component is not homogeneously redistributed back into the matrix. The maximum scattering amplitude in the Al-Sm core-shell model is always at nonzero q, regardless of the value of R_c or the concentration or distribution of Sm in the shell. In addition, the magnitude of the maximum scattering intensity depends on the radii of nanocrystal core and Sm-rich shell rather than solely on the magnitude of the contrast in densities. This difference is exploited in the analysis of particle sizes.

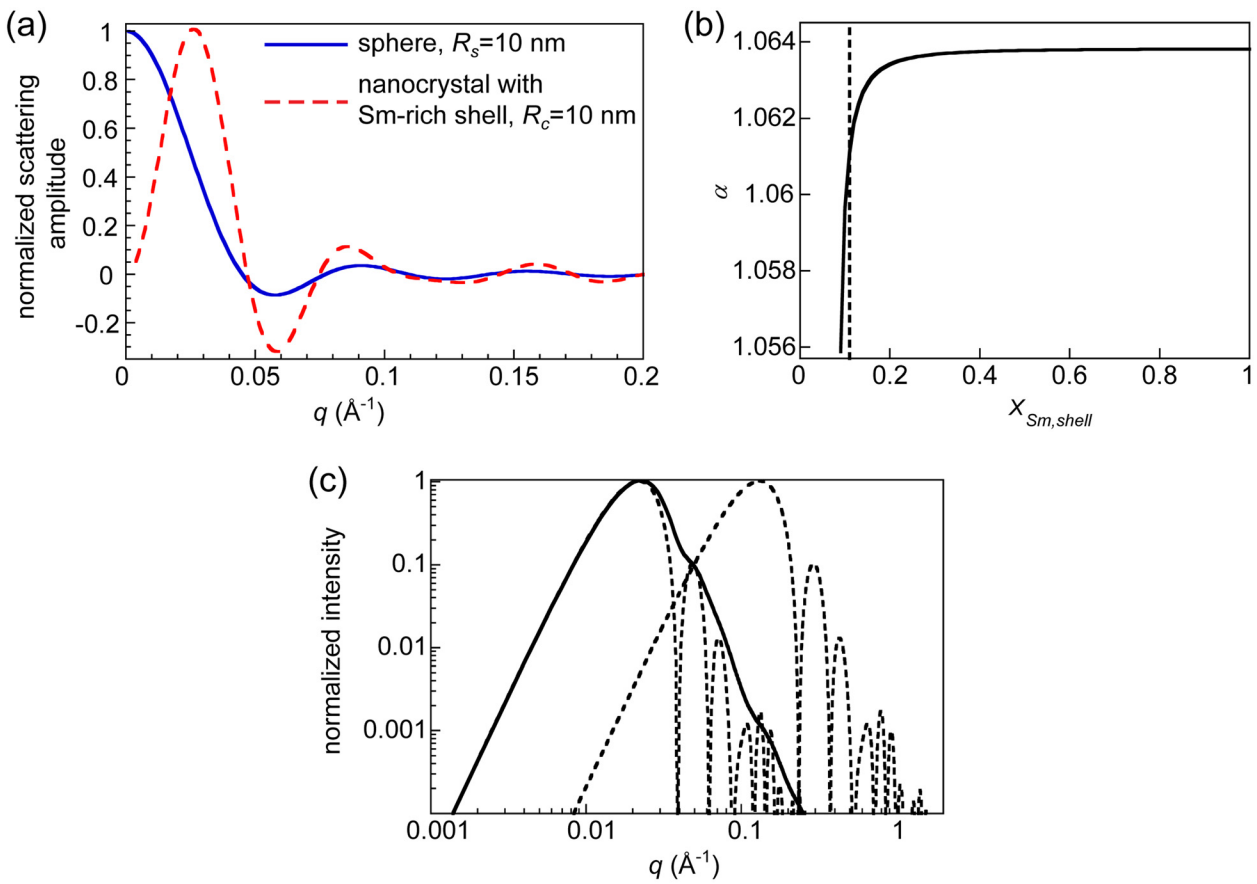

FIG. 3. (a) Amplitudes of scattering from a sphere with a radius of 10 nm (solid line) and a core-shell particle formed from an alloy with $X_{Sm,alloy} = 8\%$, with a shell with $X_{Sm,shell} = 11\%$, and a core of radius R_c=10 nm (dashed line). Each amplitude is normalized to have a peak value of 1. (b) Values of the coefficient α in equation (6) as a function of $X_{Sm,shell}$. For the expected concentration of Sm in the shell, $X_{Sm,alloy} = 11\%$ indicated by the dashed line, $\alpha = 1.061$. (c) Normalized predicted scattering intensities from models corresponding to Al nanocrystal/Sm-rich shell particles with nanocrystal radii of 2 and 12 nm (dashed lines with peaks near 0.02 and 0.2 Å^{-1}, respectively), and from a uniform distribution of particles with sizes between these extremes (solid line).

Based on a numerical study of the scattering distribution we find that the peak of the scattering amplitude occurs at $q = q_{\text{peak}}$ with

$$q_{peak} = \alpha \frac{2\pi}{R_s + R_c}. \quad (6)$$

The factor α in Eq. (6) depends only slightly on the Sm concentration in the shell. With $X_{\text{Sm,alloy}} = 8\%$, αvaries from 1.056 for small concentrations of Sm in the shell to 1.064 for large concentrations. The variation of α as a function of $X_{\text{Sm,shell}}$ is shown for $X_{\text{Sm,alloy}} = 8\%$ in Fig. 3(b). The value of α also depends slightly on $X_{\text{Sm,alloy}}$. α reaches 1.07 for small concentrations of Sm in the starting material. Thus, q_{peak} is related to the sum of the radii of the nanocrystal core and Sm-rich shell with approximately 1% accuracy.

The intensity of the x-rays scattered from each particle is proportional to $|A(q)|^2$. In the experiments reported here, x-rays are scattered in a plane perpendicular to the horizontal electric field polarization, and there is thus no need to correct for polarization effects. The intensity depends on the x-ray absorption in the sample so that the ratio of the scattered intensity to the incident intensity is $\Omega t T_s [d\Sigma(q)/d\Omega]$, where the solid angle of the detector Ω, and the thickness of the sample t are known in advance.[14] Using the x-ray transmission of the sample T_s, it is possible to make quantitative measurements of the differential scattering cross section $d\Sigma(q)/d\Omega$ from the scattered intensities. The value of $d\Sigma(q)/d\Omega$, measured in cm^{-1}, can be related to the scattering power predicted by the model using $d\Sigma(q)/d\Omega = r_0^2 I(q)$, with $I(q) = (1/V_s)|A(q)|^2$. Here V_s is the total illuminated volume of the sample and r_0 is the classical radius of the electron. $I(q)$ is the scattering power and has a value depending on the square of a number of electrons per unit volume.[11]

C. Scattering from a distribution of particles

The model describing the scattering due to a single particle can be extended to predict the intensity distribution arising from a sample in which there are a number of Al nanoparticles of different sizes. The number density and spatial distribution of nanocrystals is assumed to be sufficiently dilute that there is no long-range order between them and that the intensity scattered from each particle in the distribution can thus be treated using the model of an isolated particle developed above. In this limit, the intensities of scattered x-rays from each particle can be added to find the intensity that is observed at the detector. Observations using transmission electron microscopy show that this assumption is reasonable for the experimental conditions described below because the number density of nanocrystals is on the order of 10^{22} m^{-3}, corresponding to a separation of many particle distances. The scattering power, due to the ensemble of particles is $I_{\text{particles}}$, given by

$$I_{\text{particles}}(q) = \int_0^\infty n(R')|A(q,R')|^2 dR' \quad (7)$$

Here $A(q,R')$ is the amplitude at scattered wavevector q arising from a single particle of size R'. The distribution $n(R')$ is defined so that $n(R')dR'$ is the number of particles per unit volume with core radii between R' and $R' + dR'$.

The scattering amplitude for a particular size of Al-nanocrystal is proportional to volume of the nanocrystal and the intensity is proportional to the square of the volume. The total intensity is very strongly dependent on the largest particles present in the sample. This effect is illustrated in Fig. 3(c), in which the intensity resulting from a uniform distribution of particle sizes from 2 to 12 nm is compared to scattering from monodisperse populations of 2 nm particles and 12 nm particles. For these distributions of particle sizes, the intensity from a distribution of particles is only slightly different from the intensity that would result from the largest particles alone. It is thus relatively straightforward to identify the largest particles in a distribution from the SAXS measurements.

An additional contribution to the small angle scattering intensity arises from the roughness of the sample surface and other sources that are not related to the Al nanocrystals. This background is proportional to $q^{-\gamma}$ with $\gamma \approx 4$. During the process of fitting the model to the data, the exponent γ and the magnitude β of the intensity due to this scattering were allowed to vary and resulted in values of γ ranging from approximately 3.3 to 4.2. A constant background δ arises from the detector and other slowly varying contributions to the scattering, and is approximately independent of q. The two background terms are thus:

$$I_{\text{background}}(q) = \beta q^{-\gamma} + \delta. \quad (8)$$

In principle, the size distribution $n(R)$ could be deduced by iteratively improving the quality of the optimum fit of this model to the data. In order to simplify the fitting process, however, we assume a size distribution in which $n(R)$ has a constant value equal to N_R for values of R between the minimum and maximum radii of nanocrystals, and zero elsewhere. The two parameters of this distribution are R_{min} and R_{max}. The assumption of a constant number density between these limiting sizes is a simple approximation observed in microscopy experiments, which find a more complex size distribution that includes more small particles and fewer large particles than would be predicted by the assumption of a constant value of $n(R)$.[15]

Since the intensity is most sensitive to the largest particles in the distribution, there is little difference between using the uniform distribution that is assumed and other more complex distributions. In each case, it is only the portion of the distribution at the largest nanocrystal radii that is relevant to the fit. A second consequence of the scaling of the scattered intensity with the square of the nanocrystal volume is that it is not possible to estimate the total number of nanocrystals accurately. Even a large number of relatively small particles would do little to change the experimentally observed intensity. The total experimentally observed intensity in the small angle scattering data is interpreted using a model given by the sum of Eqs. (6) and (7), along with an assumption that $n(R)$ is uniform between the two limiting sizes.

IV. RESULTS

The fit of the scattering model described in the previous section to SAXS results for a sample heated to 120 °C for 24 h is shown in Fig. 4(a). Figure 4(a) also includes experimental results from an unprocessed sample in the same state it was formed by melt-spinning. The growth of the Al nanocrystals causes scattering from the annealed sample to be much more intense than from the as-spun ribbon in the range of q between 0.015 and 0.1 $Å^{-1}$. The maximum radius deduced from the fit of the model to the measurement with the annealed sample in Fig. 4(a) was 10 nm. The fit was not sensitive to the minimum radius, which was arbitrarily taken to be 1 nm.

The fit shown in Fig. 4(a) systematically underestimates the intensity of x-rays scattered to large values of q between 0.04 $Å^{-1}$ and 0.1 $Å^{-1}$. This mismatch is also apparent in the ratio of the observed data to the fit, shown in Fig. 4(b). This discrepancy may indicate that there are a large number of smaller particles that are not described by the uniform size distribution.

The SAXS can also be interpreted using the relationship between the radii and wavevector of the peak intensity given by Eq. (6). Using the value of α corresponding to the experimental composition, the radius R_c of the pure-Al nanocrystal core is given by

$$R_c \approx 2.65 \frac{1}{q_{\text{peak}}}. \tag{9}$$

For the value of q for which the maximum intensity is observed in Fig. 4(a), the radius from Eq. (9) is 11 nm. This is remarkably close to the value of 10 nm obtained by fitting. Both of these radii are within the uncertainty of the diameter observed in microscopy studies for the same annealing conditions.

Scattering data is shown in Fig. 5 for samples annealed at several temperatures between 120 and 140 °C. The fits shown with the data in Fig. 5 were obtained iteratively by comparing the calculation with the experimental intensities. The fit of the model is poor for as-spun ribbons, as shown in the intensity distributions in Fig. 4. Especially at low overall crystalline volume fraction, this poor fit may arise from sample artifacts unrelated to the nanocrystals, including surface roughness. In addition, the fit to the data at the earliest time point, corresponding to annealing at 120 °C for 6 h, Fig. 5(a), is not as good as for the other times and temperatures, and the maximum crystal size for this time and temperature is not included in the examination of the growth behavior in the next section. The results of the fits for all other samples are shown in Fig. 6(a).

A comparison of the sizes determined from the SAXS and size distributions measured using TEM image analysis is shown in Fig. 6(b) for samples annealed at 130 °C. The maximum size observed in TEM experiments and radii found in the SAXS measurements agree within the uncertainty of the measurement at all times.

As shown in the number density derived from TEM measurements in Fig. 7, the crystal number density rises during annealing at 130 °C until the nucleation reaction reaches saturation after approximately 3 h. Between 3 and 6 h the total number density is constant. At times longer than 6 h, the smaller nanocrystals begin to dissolve and the total number density decreases, as would be expected when coarsening dominates the particle growth. The dissolution of small particles is not visible in the SAXS results because the scattering intensity is most sensitive to the largest nanocrystal sizes, which are still growing. The key point in the comparison of TEM and SAXS data in Fig. 6(b) is that there is excellent agreement in the sizes of the largest nanocrystals.

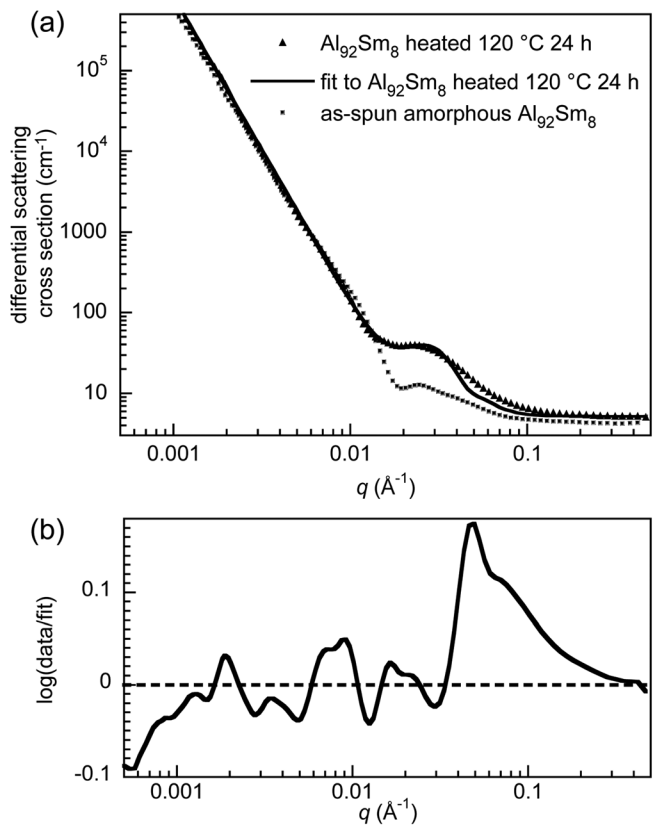

FIG. 4. (a) Small angle x-ray scattering intensities for the unprocessed amorphous mixture and a sample heated to 120 °C for 24 h. The solid line is a fit to the data using the Al-nanocrystal/Sm-rich shell model. (b) Ratio of the measured and model intensities.

V. DISCUSSION

The nanocrystal/Sm-rich shell model for the SAXS experiments allows a determination of the size of the largest nanocrystals within the population accurately and unambiguously. The nanocrystal sizes derived from the SAXS model can then be used to determine the growth mechanism by which nanocrystals grow after nucleation in complete. Extrapolating the nanocrystal sizes plotted in Fig. 6(a) to shorter annealing time shows that the nanocrystals would have been already developed relatively large radii at very early times. It is immediately apparent that the growth mode at long times is different from the fast growth during initial nucleation. Previous studies have found that the initial growth of the nanocrystals is rapid and may be achieved

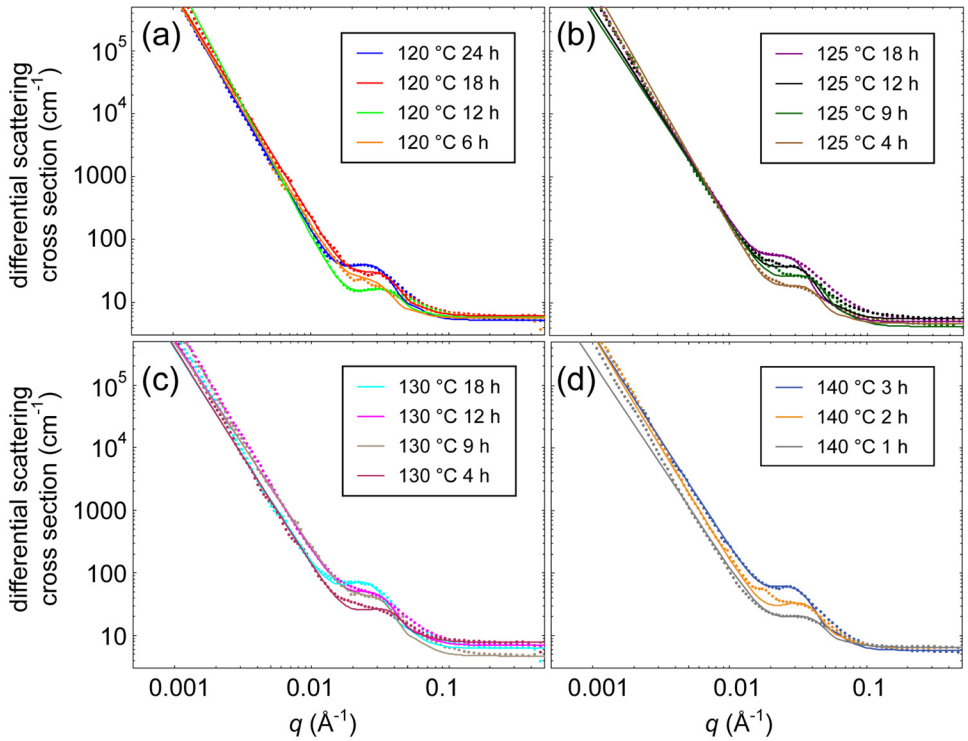

FIG. 5. Small angle scattering intensities and fits for samples processed at (a) 120 °C, (b) 125 °C, (c) 130 °C, and (d) 140 °C.

through a mixture of diffusional control and interfacial attachment. This initial period of fast growth ends after the diffusion fields of adjacent particles impinge on one another.[16]

The full range of SAXS measurements at different times and temperatures can be used gain quantitative insight into the kinetics in both late and early time regimes. At late times, once the nanocrystal number density has reached saturation and the metastable equilibrium volume fraction of Al is achieved, normal growth control ceases and the nanocrystals evolve via coarsening. For a coarsening mechanism the maximum growth rate is achieved for the particle size $\bar{R}_C$. This maximum growth rate is[17]

$$\left(\frac{dR_C}{dt}\right)_{\max} = \frac{6D\sigma X_{\mathrm{Al,shell}} V_m}{RT}\frac{1}{\bar{R}_C^2}, \tag{10}$$

where D is the diffusion coefficient for Al in the Al-Sm amorphous alloy, σ is the nanocrystal/amorphous alloy interfacial energy, $X_{\mathrm{Al,shell}}$ is the tie line atomic fraction of Al in the Sm-rich shell, the molar volume V_m is equal to $1/N_t$, and R is the gas constant. The interfacial energy at temperature T is $\sigma(T) = 0.141 + 7.952 \times 10^{-5}T$, based on the Spaepen model.[18]

Figure 8 shows a plot of the values of D obtained by applying Eq. (10) to the particle growth rates obtained from

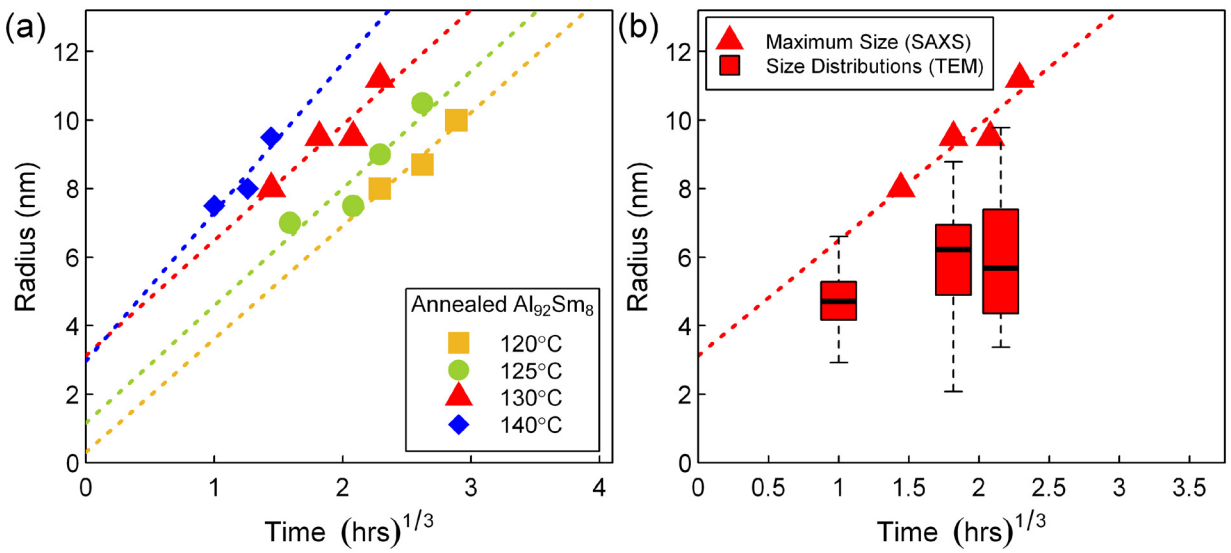

FIG. 6. (a) Maximum nanocrystal radii for samples processed at 120, 125, 130, and 140 °C. (b) Measured size distributions from TEM and the maximum radii measured by SAXS of Al nanocrystals annealed at 130 °C at several times. The TEM size distributions are plotted by indicating the mean size with a solid crossbar, the maximum and minimum sizes as horizontal lines, and boxes bounded by the intermediate quartiles of the distribution.

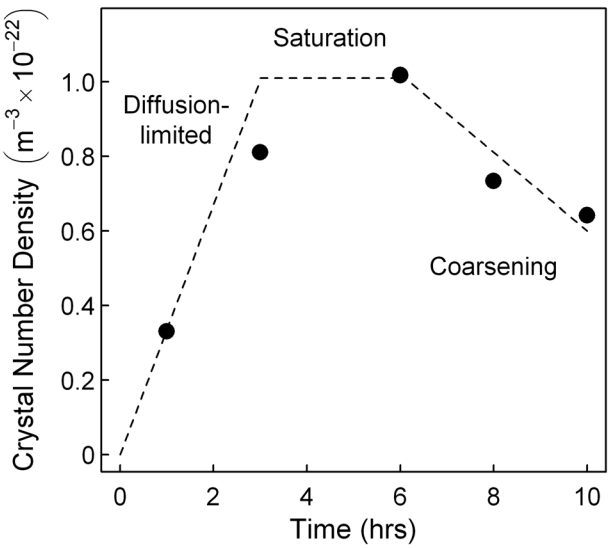

FIG. 7. Number density of aluminum nanocrystals as a function of time for $Al_{92}Sm_8$ samples annealed at 130 °C for various times, determined using TEM. The dashed lines show times at which the phenomena indicated in the labels are occurring.

SAXS measurements. The solid line in Fig. 8 is a least squares fit of an Arrhenius model for the dependence of the diffusivity on temperatures, with $D = D_0 \exp(-Q/RT)$. The fit gives $D_0 = 1.2 \pm 2 \times 10^{-7}$ m^2 s^{-1} and $Q = 1.02 \pm 0.1 \times 10^5$ J mol^{-1}. These transport parameters are obtained using only the maximum radii found by SAXS.

A comparison can now be made between the coarsening model for the SAXS measurements and the full particle distribution obtained at a single temperature using TEM. The predicted growth rate for particles of any size is

$$\frac{dR_C}{dt}(R_C) = \frac{2D\sigma X_{\mathrm{Al,shell}} V_m}{RTR_C}\left(\frac{1}{\bar{R}_C} - \frac{1}{R_C}\right). \qquad (11)$$

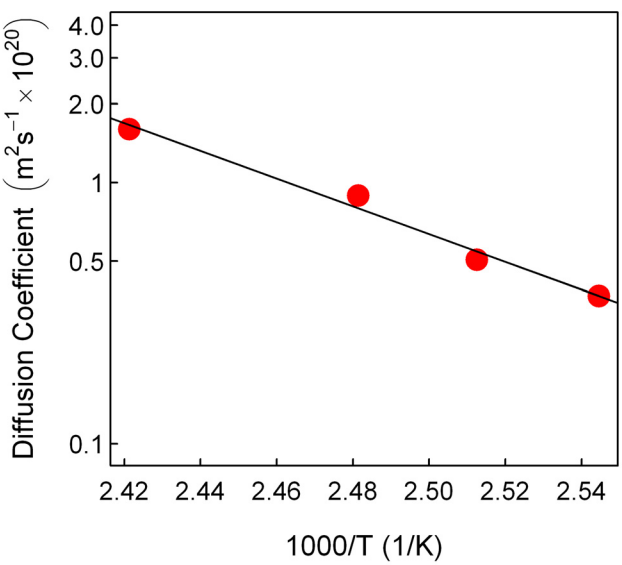

FIG. 8. Diffusion coefficient for Al in the Al-Sm amorphous alloy as a function of temperature, as calculated by assuming a coarsening model during long time annealing.

The size ranking of each particle, i, is considered to be preserved between annealing times. Thus largest crystal at time t_1 is also the largest crystal at a later time t_2. Therefore, $\Delta R_i/\Delta t$ is the growth rate for the particle with size ranking i.

The growth rates determined from TEM analysis are shown as the data points in Fig. 9 for the ribbon annealed at 130 °C. The growth rate was measured as a function of particle size for two time steps: between 1 and 6 h and between 6 and 10 h. In the first time range the growth rate is positive for all particle sizes. At later times, the growth rate is positive for large particles, but negative for smaller particles. At this later stage, the smaller Al nanocrystals are thus dissolving and transferring Al to the larger particles. The trend in growth rates observed in Fig. 9 is consistent with a coarsening mechanism.

A further quantitative comparison can be established between the coarsening model and the sizes determined using TEM. The velocities predicted using the coarsening model are shown as the solid line for later-time and larger size data in Fig. 9. The diffusion constant for this prediction is derived from the SAXS measurements. The agreement between the TEM data and the prediction made from analysis of the SAXS results confirms that the diffusion coefficient obtained from the coarsening model is accurate.

The diffusion coefficient determined from the long annealing time can now be used to gain insight into the growth process at shorter times. As shown in Fig. 9, the growth rates of the smaller particles at shorter times are positive over the entire range of sizes in the interval between 1 and 6 h. This result coincides with previous experience that growth is initially fast and that the growing solute shell layer surrounding the crystal impedes growth by limiting the diffusion of Al to the nanocrystal.[16] When growth rates are limited by the diffusion of Al through the Sm-rich shell surrounding the Al nanocrystal, the rate of change of the radius

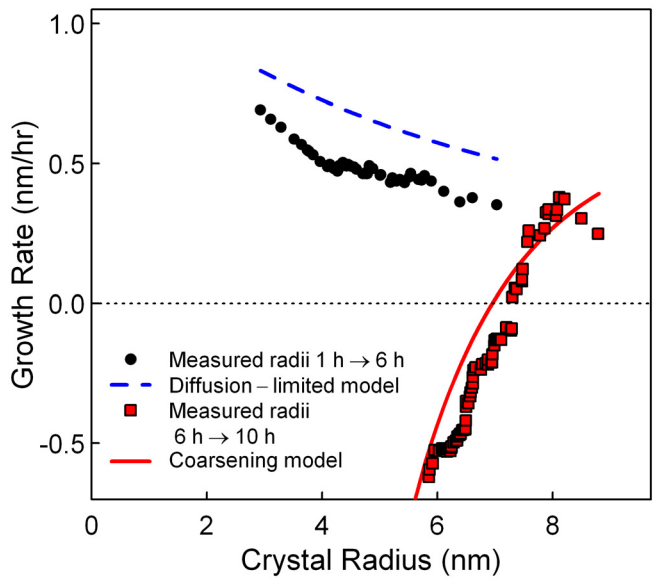

FIG. 9. Growth rate dR_c/dt during annealing at 130 °C determined using TEM for several sizes of nanoparticles for two time intervals, between 1 and 6 h (black circles) and between 6 and 10 h (squares). The lines are fits of a coarsening model (solid line) at long times, and a diffusion controlled growth model at earlier times (dashed line).

for all nanocrystal sizes can be expressed in a simplified form by

$$dR_C/dt = (\alpha_3/2)\sqrt{D/t}. \quad (12)$$

where the diffusion coefficient for Al through the Sm-rich shell is taken to be the same as it is in the Al-Sm amorphous alloy. Equation (12) applies to noninteracting particles, as expected at early times and treats growth under a local interfacial equilibrium. The coefficient α_3, depends on the concentration of Al in the nanocrystal $X_{\mathrm{Al,NC}}$, the concentration in the shell $X_{\mathrm{Al,shell}}$, and the concentration in the matrix, $X_{\mathrm{Al,alloy}}$.[19]

$$\alpha_3 = \sqrt{3}\frac{X_{\mathrm{Al,alloy}} - X_{\mathrm{Al,shell}}}{\sqrt{X_{\mathrm{Al,NC}} - X_{\mathrm{Al,shell}}}\sqrt{X_{\mathrm{Al,alloy}} - X_{\mathrm{Al,shell}}}}. \quad (13)$$

Equation (13) predicts $\alpha_3 = 0.55$. The prediction of the diffusion limited growth rates from Eq. (12) is plotted as a dashed line in Fig. 9. The predicted growth rate exceeds the observed growth rate by a factor of ~1.5, but the overall trend is similar indicating that the diffusion limited growth mechanism applies at early times prior to the kinetic transition to coarsening.

VI. CONCLUSION

The small angle scattering method and data presented here provide new insight into the growth of Al nanocrystals in Al-Sm alloys. The SAXS measurements agree with TEM particle counting measurements of primary crystallization particle sizes. Furthermore, a distinct change is observed in the growth behavior as a function of time corresponding to a change in the mechanism of nanocrystal growth from diffusion-limited growth to coarsening. The SAXS measurement of the largest nanocrystal sizes within these materials during coarsening is an excellent match for the problem understanding the dynamics in the coarsening regime, where the largest nanocrystals are particularly important.

Based on the experimental results, the following physical picture is proposed to explain the evolution of the growth mode of the nanocrystals during annealing. At the earliest times, there is a relatively low overall transformed volume. This translates into a longer diffusion path between particles and a matrix composition which still contains a supersaturation of Al atoms. The subsequent saturation of the number density occurs because the growing nanocrystals deplete aluminum from amorphous Al-Sm alloy and reduce the supersaturation. Later, the nanocrystals cannot grow independently, due to the impingement of the diffusion fields of nearby crystals. Finally, once a metastable equilibrium is reached between the amorphous Al-Sm alloy and the nanocrystals, the overall free energy is reduced via coarsening through growth of the largest crystals at the expense of the smallest.

ACKNOWLEDGMENTS

PGE acknowledges support from the NSF through the University of Wisconsin Materials Research Science and Engineering Center (NSF DMR-1121288). SDI and JHP gratefully acknowledge support by NSF (DMR-1005334). Use of the Advanced Photon Source was supported by the U.S. Department of Energy, Office of Science, Office of Basic Energy Sciences, under Contract No. DE-AC02-06CH11357. The authors acknowledge most helpful conversations with Dr. Masato Ohnuma of the National Institute for Materials Science, Tsukuba, Japan on the core shell model. We thank D.-H. Do, W. S. Tong and J. A. Hamann for their assistance in obtaining the results used in this analysis.

[1]A. Inoue, Prog. Mater. Sci. **43**, 365 (1998).
[2]D. V. Louzguine-Luzgin and A. Inoue, J. Mater. Res. **21**, 1347 (2006).
[3]P. Bruna, E. Pineda, and D. Crespo, J. Non-Cryst. Solids **353**, 1002 (2007).
[4]J. Antonowicz, M. Kedzierski, E. Jezierska, J. Latuch, A. R. Yavari, L. Greer, P. Panine, and M. Sztucki, J. Alloys Compd. **483**, 116 (2009).
[5]J. H. Perepezko, R. J. Hebert, W. S. Tong, J. Hamann, H. R. Rosner, and G. Wilde, Mater. Trans. **44**, 1982 (2003).
[6]U. Bonse and M. Hart, Appl. Phys. Lett. **7**, 238 (1965).
[7]J. Ilavsky, P. R. Jemian, A. J. Allen, F. Zhang, L. E. Levine, and G. G. Long, J. Appl. Crystallogr. **42**, 469 (2009).
[8]G. G. Long, P. R. Jemian, J. R. Weertman, D. R. Black, H. E. Burdette, and R. Spal, J. Appl. Crystallogr. **24**, 30 (1991).
[9]H. Hermann, A. Wiedenmann, and P. Uebele, J. Phys. Condens. Matter **9**, L509 (1997).
[10]U. Lembke, R. Brückner, R. Kranold, and Th. Höche, J. Appl. Crystallogr. **30**, 1056 (1997).
[11]A. Guinier, *X-ray Diffraction in Crystals, Imperfect Crystals, and Amorphous Bodies* (Freeman, New York, 1963).
[12]J. S. Pedersen, Adv. Colloid Interface Sci. **70**, 171 (1997).
[13]B. Boucher, P. Chieux, P. Convert, and M. Tournarie, J. Phys. F **13**, 1339 (1983).
[14]P. Jemian, Ph.D. thesis, Northwestern University (1990).
[15]J. H. Perepezko, R. J. Hebert, and G. Wilde, Mater. Sci. Eng., A **375–377**, 171 (2004).
[16]D. R. Allen, J. C. Foley, and J. H. Perepezko, Acta Mater. **46**, 431 (1998).
[17]G. W. Greenwood, Acta Metall. **4**, 243 (1956).
[18]F. Spaepen, Solid State Phys. **47**, 1 (1994).
[19]C. Zener, J. Appl. Phys. **20**, 950 (1949).